

A Computationally Efficient Hybrid Neural Network Architecture for Porous Media: Integrating CNNs and GNNs for Improved Permeability Prediction

Qingqi Zhao¹, Xiaoxue Han², Ruichang Guo¹, Cheng Chen^{1*}

¹ Department of Civil, Environmental and Ocean Engineering, Stevens Institute of Technology, Hoboken, NJ, USA

² Department of Computer Science, Stevens Institute of Technology, Hoboken, NJ, USA

* Corresponding author: Cheng Chen (cchen6@stevens.edu)

Abstract

Subsurface fluid flow, essential in various natural and engineered processes, is largely governed by a rock's permeability, which describes its ability to allow fluid passage. While convolutional neural networks (CNNs) have been employed to estimate permeability from high-resolution 3D rock images, our novel visualization technology reveals that they occasionally miss higher-level characteristics, such as nuanced connectivity and flow paths, within porous media. To address this, we propose a novel fusion model to integrate CNN with the graph neural network (GNN), which capitalizes on graph representations derived from pore network model to capture intricate relational data between pores. The permeability prediction accuracy of the fusion model is superior to the standalone CNN, whereas its total parameter number is nearly two orders of magnitude lower than the latter. This innovative approach not only heralds a new frontier in the

research of digital rock property predictions, but also demonstrates remarkable improvements in prediction accuracy and efficiency, emphasizing the transformative potential of hybrid neural network architectures in subsurface fluid flow research.

Introduction

Subsurface fluid flow is prevalent in numerous natural and industrial processes, including contaminant transport, nuclear waste disposal, and geological carbon sequestration¹⁻³. A key parameter governing these processes is the rock permeability, which describe the rock's capability to allow a fluid to flow through it. Rock permeability can be determined using experiments based on Darcy's law. However, these experiments are not only time-consuming but also substantially limited by laboratory conditions. Conducting them on a large scale becomes impractical due to the extensive time involved. Recent advancements in imaging technologies, such as micro-computed X-ray tomography, have enabled the visualization of porous media's internal structure in three dimensions (3D) and facilitated the characterization of their physical properties through numerical simulations^{4,5}. Nonetheless, directly simulating flow within 3D porous media remains computationally demanding, even when employing parallel computing techniques^{6,7}.

The recent advancements of neural networks have significantly propelled research in pattern recognition and image segmentation^{8,9}. Deep learning technology, particularly convolutional neural network (CNN), present a promising method for estimating permeability efficiently and accurately¹⁰⁻¹⁵. In previous studies, CNNs have been the primary choice for image-based permeability prediction, with the variance of model architecture or adding physics information to

enhance prediction accuracy¹⁶⁻¹⁹. While CNNs can be seen as tools that automatically identify geometric features, they can lose certain details during the convolution process with activation functions¹⁷. Furthermore, CNNs are primarily designed for regular Euclidean data like images (2D grids) or texts (1D sequences). Adapting CNNs to non-Euclidean domains presents challenges, especially in defining localized convolutional filters and pooling operators. Addressing these challenges, geometric deep learning, especially deep learning on graphs, has gained momentum as an emerging research area²⁰.

One such advancement in addressing these challenges is the development of graph neural network (GNN), a specialized neural network designed for graph data structures²¹⁻²⁵. They were developed in response to the difficulties encountered by traditional CNNs when dealing with the unconventional sizes and complex structures of graphs. GNNs are adept at capturing the complex relationships between nodes in a graph, leading to significant advancements in graph analysis research. Their applications include a wide range of tasks, such as graph classification, link prediction, community detection, and graph embedding²⁶. Recently, GNNs have risen in popularity across various domains, from social networks and recommender systems to life sciences and biomedical engineering. In molecules property prediction, for example, graph architecture is naturally aligned with the input representations of molecules and materials, which can be viewed as chemical graphs of atoms and bonds²⁷. This alignment allows GNNs to access comprehensive atomic-level material representations²⁸. Coupled with their flexibility to incorporate physical laws and larger-scale phenomena, GNNs can develop detailed material representations useful for specific tasks, like predicting material properties²⁹. As a result, GNNs offer a promising alternative to traditional feature representations commonly used in the natural sciences.

Despite the potential of GNNs, their application in predicting porous media properties has not been extensively explored in previous research. This work pioneers the utilization of porous media graph structures extracted from digital rock images through pore network modeling (PNM). Subsequently, we constructed a GNN model that utilizes digital rock graphs as inputs to predict permeability. Through a comparative visualization of the importance scores between CNN and GNN predictions, we illuminate the potential shortcomings of CNN in permeability prediction and highlight how the GNN addresses these challenges. Building on the strengths of both CNN and GNN, we present a novel fusion model designed for enhanced multiscale feature extraction of porous media. This study represents the first comprehensive exploration of using a GNN model for digital rock property prediction. Notably, our fusion model of GNN and CNN exhibits a marked improvement in prediction accuracy and demonstrates considerable benefits in computational memory efficiency.

Results

Data extraction and structure

Most of the research on implementing deep learning technology for predicting digital rock properties is based on CNN models¹⁶. CNNs are well-suited to deal with problems related to spatial correlations due to their ability to recognize shift-invariance, local connectivity, and compositionality of image data²⁰. As illustrated in Fig. 1a, a CNN framework for the analysis of digital rock data typically uses images as input, represented as regular grids in Euclidean space. By this method, CNNs can extract local meaningful features that are shared with the entire data sets for the analysis of porous media images. A challenge for CNNs is the increased

computational and memory demands during training, especially for large 3D images, where the escalating number of pixels significantly increases memory usage, consequently diminishing the model's computational speed. Numerous studies have highlighted the constraints of current computational resources in forecasting rock characteristics via CNNs^{16,18}.

Porous media can be considered as a kind of graph due to their pore-throat-pore connection relationship. While CNNs can effectively capture hidden patterns of Euclidean data, the complexity of graph data has imposed significant challenges on the existing machine learning algorithms. GNNs, on the other hand, utilize distinct methodologies for data analysis in comparison to the CNN model. For digital rock studies, rather than examining digital rock at the pixel level, GNNs convert the digital rock images into graph formats representing the pore and throat structure by nodes and edges (Fig. 1b). This transformation can scale up the input data from the pixel level (images) to the pore-scale level (pore network), which significantly reduces the memory consumption and accelerates training. Given that graphs can be irregular, each graph may have a different number of nodes, and within a graph, individual nodes can have varying numbers of neighbors. Such flexible data structure endows the GNN with a more adaptable data input dimension, eliminating the need for fixed input data dimensions as seen in CNNs. Furthermore, a core assumption of existing CNN models is that instances (e.g., pixels in the digital rock images) are independent of each other. This assumption is no longer applicable to graph data because instances (e.g., nodes in the digital rock graphs) are interconnected by graph edges (e.g., throats). Additionally, the graph structure's selective emphasis on key features facilitates quicker data retrieval and processing, making it a more streamlined and efficient storage alternative to pixel-level images. This representation allows GNNs to focus on the connectivity and relationships within the data, which is crucial for understanding the complexity

of the pore structure. In this study, the PNMs were derived from digital rock images. The pore network is a widely used conceptual framework in the study of porous media that provides a simplified representation of the complex microscopic architecture³⁰. Data regarding the pore sizes, throat lengths, and other geometric and physical properties is generally stored in structured arrays or matrices. These extracted PNMs were utilized to construct graphs, with pores represented as nodes and throats as edges. Essential attributes such as the pore diameter were computed during this extraction process and assigned as labels to the nodes. Similarly, parameters including throat diameters were measured and set as labels for the edges. The details of the graph attributes are provided in the Method section.

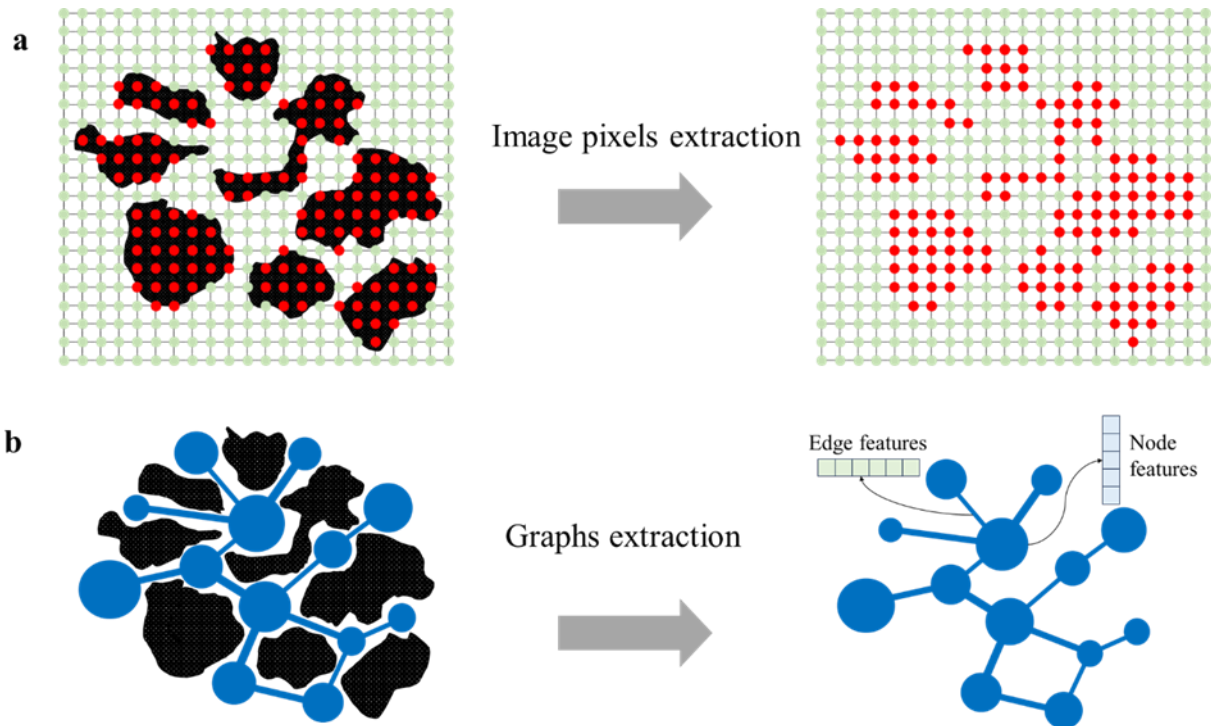


Fig. 1. Illustration of data extraction from digital rock utilizing convolutional and graph neural networks. a Pixel extraction from a digital rock image. **b** Graph extraction from a PNM, with the node and edge features sourced from PNM calculations.

A dataset from DeePore provided 17,700 semi-realistic 3D microstructures of porous geomaterials, each with a resolution of 256^3 voxels³¹. These images were used as the inputs to CNNs, and their extracted graphs were subsequently employed as the inputs to the GNN. The dataset was derived from the original core of 60 real micro-tomography images of porous materials. Due to the need for a large and diverse dataset for optimal deep learning training, and the limited availability of varied tomography data, data augmentation techniques were employed. A texture interpolation technique was adopted where two images from the core dataset are combined to create a hybrid texture through weighted averaging of normalized distance maps. To ensure diversity and realism in the augmented dataset, random shifts and translations were introduced to the interpolated textures. The generated dataset was further refined by excluding outlier geometries with non-physical properties that are unsuitable for regression modeling. Additionally, the dataset features 30 physical properties of each sample calculated using physical simulations on the corresponding PNMs. For our study, we utilized the permeability values from this physical property dataset as the ground truth for our deep learning models. The lengths within this dataset are measured in pixels (px). As a result, permeabilities for all synthetic geometries are reported in pixel squared units (px^2). The rescaled permeability value can be determined by multiplying the reported permeability in px^2 by the square of the spatial resolution.

The construction of the deep learning models

We implemented and compared two CNN architectures: the 2DCNN and the 3DCNN, both structured with three convolutional layers that increase in channel numbers for capturing intricate data representations. Subsequent to these layers, max-pooling is employed for down-sampling

and achieving translational invariance. The output is then flattened, followed by dropout for regularization and fully connected layers to deduce the final permeability prediction.

The primary distinction between the two CNN models lies in their input data dimensions. For the 3DCNN, we utilized the original 256^3 voxel images. In contrast, the 2DCNN model transforms 3D images into synthetic RGB images. Three perpendicular mid-planes are extracted from the 3D data, from which distance transforms are computed for both solid and void areas. This results in three feature maps, which not only encapsulate the original binary representation but also measure the shortest distance to the nearest boundary. These three-channel 2D images are similar in structure to common RGB images. Despite the fact that these images have three channels, their spatial dimensions remain 2D. Therefore, we refer to our model as a '2DCNN' to distinguish it from traditional 3D CNNs, which are designed to handle truly 3D data, such as the $256 \times 256 \times 256$ voxel images used in our 3DCNN model.

Additionally, we constructed a GNN model that processes graphs extracted from the 3D images. This model employs graph convolution layers to transform features, aggregates node and edge attributes into a graph-level representation, and refines this through a multi-layer perceptron for predicting permeability. The details of the CNN and GNN model architectures are provided in the Method section.

Following the development of the GNN and 2DCNN models, we introduced a fusion model, named GNN-2DCNN, which seamlessly integrates the capabilities of both architectures (Fig. 2). Fusion models, which merge multiple input sources or different feature representations, have made significant process in computer vision applications, especially in scenarios involving multimodal images or different image sensors²⁷. Such fusion techniques exploit the complementary nature of multiple feature representations, providing a more comprehensive

insight into the data. Furthermore, by merging different representations or modalities, fusion models increase robustness and reduce the uncertainty inherent in each individual representation. Based on these advantages, our proposal is a hybrid neural network that merges feature representations from the separately trained GNN and 2DCNN models. While the GNN is designed to handle node and edge features of graphs, the 2DCNN specializes in processing pixel-level images. After processing their respective inputs, the resulting outputs from both models are concatenated and then passed through dense layers for the final permeability prediction.

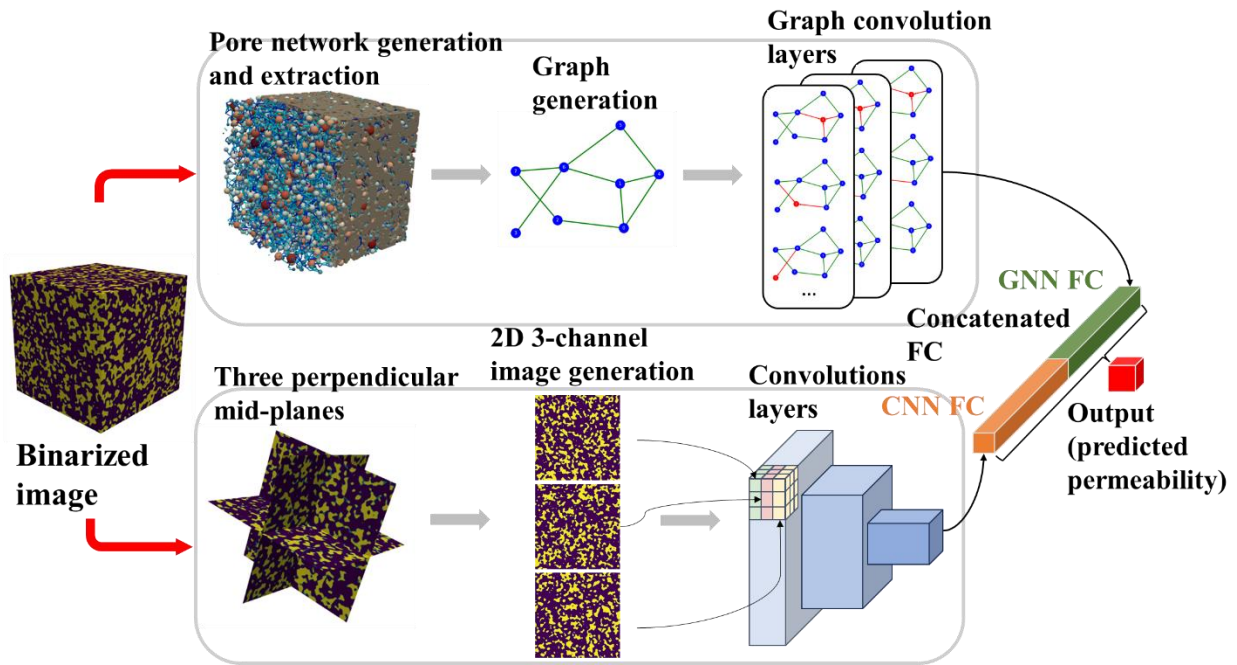


Fig. 2. Schematic diagram of the fusion model that integrates GNN and 2DCNN.

Model performance comparison

To evaluate the performance of different deep learning models — 2DCNN, 3DCNN, GNN, and the GNN-2DCNN fusion model — in predicting rock structures, a testing dataset comprising of

1,770 rock images from DeepPore³¹ was utilized. Two metrics, the R^2 score and the mean squared error (MSE), were used to quantify model accuracy. The results of the models' accuracy and efficiency are presented in Table 1 and Table 2, while Fig. 3 provides a visual representation of each model's performance.

The 2DCNN model, unfortunately, underperformed with an R^2 score of 0.82 and the highest MSE of 0.164. This performance decrement can be attributed to the significant loss of information incurred during the conversion of original 3D images to a compressed 2D format, which undermines the predictive accuracy of the model. Surprisingly, even though the 2DCNN had a greater number of trainable parameters (798,325) than the GNN, it had a shorter training time per epoch (3.84 seconds). This could be due to the fact that graph-based operations in the GNN, which involve adjacency matrices and node features, can be computationally intensive. In contrast, the 3DCNN, which utilizes the original 3D images, demonstrated significantly improved prediction performance, with a higher R^2 score of 0.94 and a reduced MSE of 0.053. However, this increased accuracy comes at a trade-off in efficiency, as evidenced by the 3DCNN model requiring a substantial 50,342,629 learnable parameters, taking up to 574.74 seconds for training per epoch, and consuming 1643 MB of GPU memory per epoch.

In comparison, the GNN model stands out with its impressive efficiency. With an R^2 score of 0.92 and only requiring 7.85 seconds per epoch for training, it not only surpassed the 2DCNN but also approached the performance level of the 3DCNN. Remarkably, this high accuracy was achieved with only 9,248 learnable parameters and a minimal GPU memory usage of 1.138 MB per epoch, emphasizing the GNN model's superior efficiency in prediction tasks. The crowning achievement was observed in the GNN-2DCNN fusion model, which combined the strengths of both architectures to yield the highest accuracy among the competitors, with an R^2 score of 0.95,

a training time of 16.86 seconds per epoch, and the lowest MSE of 0.048. Despite possessing 812,692 trainable parameters, almost similar to the 2DCNN, the fusion model expertly exploited the different feature representations intrinsic to both the GNN and CNN models. This collaborative integration of features, which are based on both digital rock images and graphs, notably improves the accuracy of permeability predictions, presenting a valuable approach for further research and practical applications.

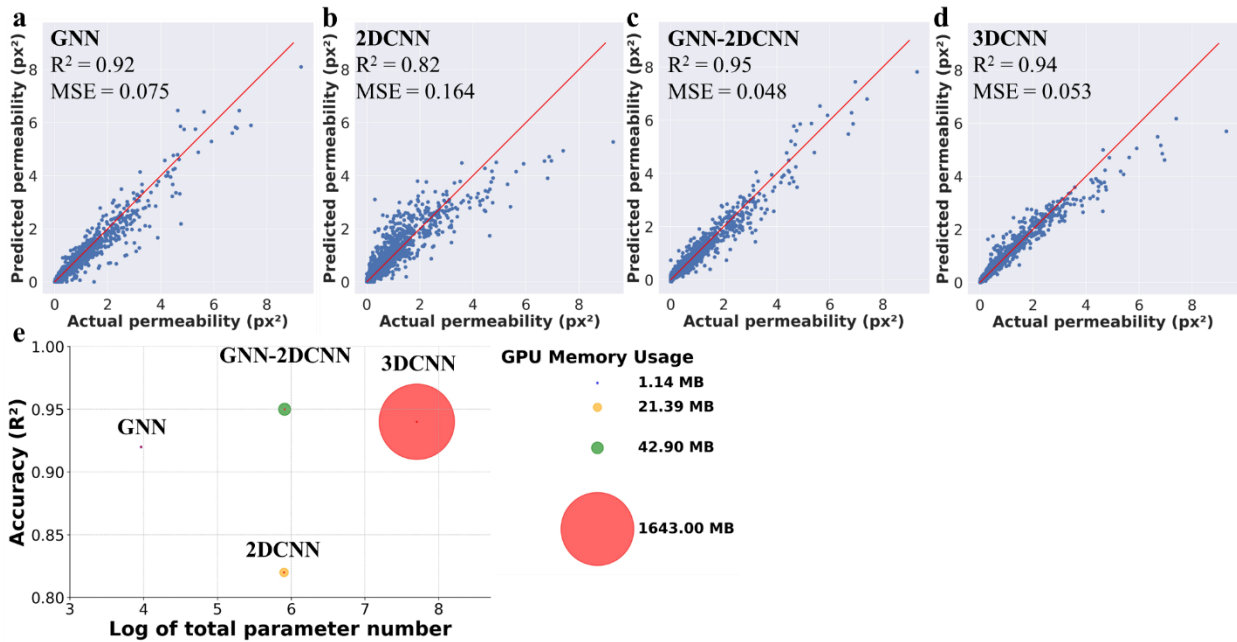


Fig. 3. Performance and efficiency comparisons between GNN, 2DCNN, GNN-2DCNN, and 3DCNN in permeability prediction. a GNN predictions. **b** 2DCNN predictions. **c** GNN-2DCNN predictions. **d** 3DCNN predictions. **e** Accuracy plotted against the log of total parameter number for each model; circle size indicates GPU memory usage.

Table 1 Computational Accuracy of Various Neural Network Models

Model	R^2	MSE
-------	-------	-----

GNN	0.92	0.075
2DCNN	0.82	0.164
GNN-2DCNN	0.95	0.048
3DCNN	0.94	0.053

Table 2 Computational Efficiency of Various Neural Network Models

Model	Training time/epoch (s)	Total trainable parameter number
GNN	7.85	9,248
2DCNN	3.84	798,325
GNN-2DCNN	16.86	812,692
3DCNN	574.74	50,342,629

Model evaluation

The comparisons of the model performance indicate that GNN and CNN have varying prediction accuracies given different data structures as inputs. To find the mechanism of the accuracy difference between GNN and CNN model, we generated 5000 2D porous media images. Of these images, 80% were utilized as the training set, 10% constituted the validation set, and the remaining 10% were allocated to the testing set. We opted for 2D images in our model evaluation as they provide a clearer demonstration of the underlying mechanisms behind CNN and GNN permeability predictions, highlighting the distinct differences in their methodologies. It is imperative to acknowledge that in nature, all rock materials inherently possess a 3D structure.

We utilized the Gradient-weighted Class Activation Mapping (Grad-CAM)³² technique to visualize the influential regions in rock images for the CNN model and significant nodes for the

GNN model that affect permeability predictions. For CNNs, Grad-CAM generates heatmaps, with warmer colors marking high-impact regions and cooler colors indicating less influential areas. Conversely, in the GNN model, an adapted version of Grad-CAM was employed, focusing on the significance of individual nodes within a graph. It resulted in the creation of a ‘node map’, highlighting the pivotal nodes influencing the permeability prediction. The goal of applying Grad-CAM is to provide a clearer understanding of how the models discern features essential for their decisions. The detailed description of the Grad-CAM methodology implemented with the CNN and GNN is provided in the Method section.

An original 2D image of a porous medium was analyzed, as shown in Fig. 4a, possessing a permeability of 2.86 darcies. Predictions from the CNN and GNN models were 5.52 and 2.85 darcies, respectively. This indicates that the GNN predicted the permeability of this digital rock more accurately than the CNN. To find the reason of it, the Grad-CAM results for CNN and GNN models were calculated as illustrated in Fig. 4b and c. In the Fig. 4b, it is evident that CNN assigns high scores to the pores in the top right corner of the porous medium (as indicated by the yellow circle in Fig. 4b), suggesting that these pores significantly influence the CNN's prediction result. However, these pores are not interconnected with the main pore network, implying that they would not facilitate flow during permeability calculations. As a result, these disconnected pores cause the CNN to overestimate the total active pore space, leading to an inflated prediction. On the other hand, the GNN Grad-CAM result in Fig. 4c within the yellow circle displays no nodes in the top-right corner, corresponding to the same location analyzed in the CNN case in Fig. 4b. The absence of nodes in the GNN visualization occurs because the PNM extraction process removes these disconnected pores to ensure a fully connected network.

Consequently, the GNN accurately identifies and considers only the active and connected pores, enhancing the precision of its predictions.

We then investigate which specific areas within a digital rock the CNN and GNN models focus on while making predictions. For a more detailed analysis, we focused on the top-left section of the digital rock sample 1, as depicted in Fig. 4a, 4b, and 4c. To give a better visualization of the CNN Grad-CAM, we overlaid the original porous media's boundary — distinguishing between the solid (black color) and void (white color) — onto the zoomed-in CNN Grad-CAM (Fig. 4b). Fig. 4b shows that the highest intensity, which denotes greatest importance scores, are given in the center of the pore space. The closer the area is to the boundary, the lower the intensity, which means CNN considers this part as less important. The CNN Grad-CAM suggests that it believes that the impact of a region on the results depends on its distance from the center of the pore. The uniform intensity in the pore space of CNN Grad-CAM indicates that CNN model might struggle to learn from the complex porous media features that characterize pore interaction, such as the pore connectivity — the number of neighboring pores connected to a particular pore. On the other hand, the zoom-in GNN Grad-CAM, which is shown in Fig. 4c, gives a clear relationship between the pore connectivity and the intensity of the importance. In this detailed representation, six nodes were specifically selected for examination. Their intensity, representing the significance each node holds, is computed from normalized GNN Grad-CAM scores. Notably, the richer the color, the more influential the node is on the GNN's final prediction. Upon closer inspection, node 1 stands out with the strongest intensity. It is surrounded by five neighboring nodes, of which three have an intensity no less than 0.4. Determining this node intensity isn't straightforward; it's influenced by multiple factors. This includes the connectivity of the pore, its inherent properties including the pore size, and the

unique properties of its adjacent pores. As an illustrative point, nodes 5 and 6, despite being similar in size to node 1, have less intensity than it. This can be attributed to the fact that node 5 is connected to only two neighbors, and the neighbors of node 6 have a less significant role than those of node 1. In a comparative light, nodes 2, 3, and 4 present with intermediate intensities, which can be ascribed to their comparatively smaller dimensions and other intrinsic properties.

Even though the six pores circled by boxes in Fig. 4c have the similar pore volume or connectivity, the color of them are different, implying that the GNN model assigns different levels of importance to them for the prediction. This variation certifies that GNN is able to evaluate the contributions of different pores on the prediction, depending on the pore's connectivity, the pore itself, and the properties of the connected pores. This ability is enabled by the message-passing mechanism of GNN:

$$h_v^{(l+1)} = \sigma \left(\sum_{u \in N(v)} W \cdot h_u^{(l)} \right) \quad (1)$$

where h represents node features, $N(v)$ are the neighbors of node v , W is a learnable weight matrix, and σ is the sigmoid activation function. By this way, GNN can comprehend the relationships between each pore and its neighbors, facilitating an understanding of flow pathways, connectivity, and pore interaction. The GNN's ability to learn porous media features like pore connectivity, may be something that CNN lacks.

The Kozeny-Carman equation has been broadly utilized in permeability prediction³³:

$$k = \frac{c_0 \phi^3}{s^2 (1 - \phi)^2} \quad (2)$$

where k is the permeability, c_0 is the Kozeny constant, \emptyset is the porosity, and s is the specific surface area. The Kozeny-Carman equation is commonly used for sandstone due to the approximation of its pore structure as a stack of spherical grains, in line with the equation's underlying assumptions. Interestingly, The CNN model shows a great ability to predict rock permeability in previous works, particularly with databases primarily composed of sandstone samples^{10,11,17,18}. The impressive accuracy of CNN models for sandstone permeability prediction may due to their capability to identify and integrate crucial high-level features like porosity and specific surface area. These features significantly influence rock permeability, as highlighted by the Kozeny-Carman equation. The effectiveness of CNNs in learning about porosity and specific surface area can be attributed to its robust image recognition and segmentation abilities. While porosity and specific surface area can generally predict permeability to a certain extent due to their connection to the Kozeny-Carman equation, other characteristics also impact permeability and can cause fluctuations. The accuracy of CNN predictions decreases when applied to rocks other than sandstones, such as carbonates¹⁰. Unlike sandstones, these rocks may have more complex structures. As a result, the straightforward relationship between permeability and the features of porosity and specific surface area breaks down; additional factors must be taken into account to improve prediction accuracy for these complex structures. To illuminate this concept further, we selected two additional 2D porous media images (shown in Fig. 4d and 4g) along with their corresponding CNN and GNN Grad-CAM results (Fig. 4e, 4f, 4h, and 4i). These two samples present similar porosity (65.26% and 65.29%, respectively) and share an identical specific surface area ($0.05 \mu m^{-1}$). We also confirm there is no disconnected pore for these two cases. Given a comparable \emptyset and s , the CNN gives similar predictions for both cases: 4.03 darcies for the first and 3.95 darcies for the second. However, the ground truths show that those

two samples have a permeability difference, with the first one 4.01 darcies and the second one 5.13 darcies. The close predictions by the CNN may result from the similarity of these two samples. Given the similar global features, ϕ and s , with similar local features, such as the pore shape, which can be detected by CNN convolution kernels, the CNN model shows a limitation to tell the difference between the two samples. On the other hand, GNN shows a more accurate prediction results, with the first one 4.07 darcies and the second one 5.23 darcies. The main reason GNN provides different predictions for these two samples is that, despite their similar ϕ and s values, they have distinct pore connectivities. The overall pore connectivity is 2.58 for the first one and 2.68 for the second one. Higher connectivity facilitates increased flow mobility, resulting in greater permeability. This implies that GNNs have the potential to recognize and account for complex pore characteristics, such as pore connectivity, through their message passing mechanism, which confers an advantage over CNNs.

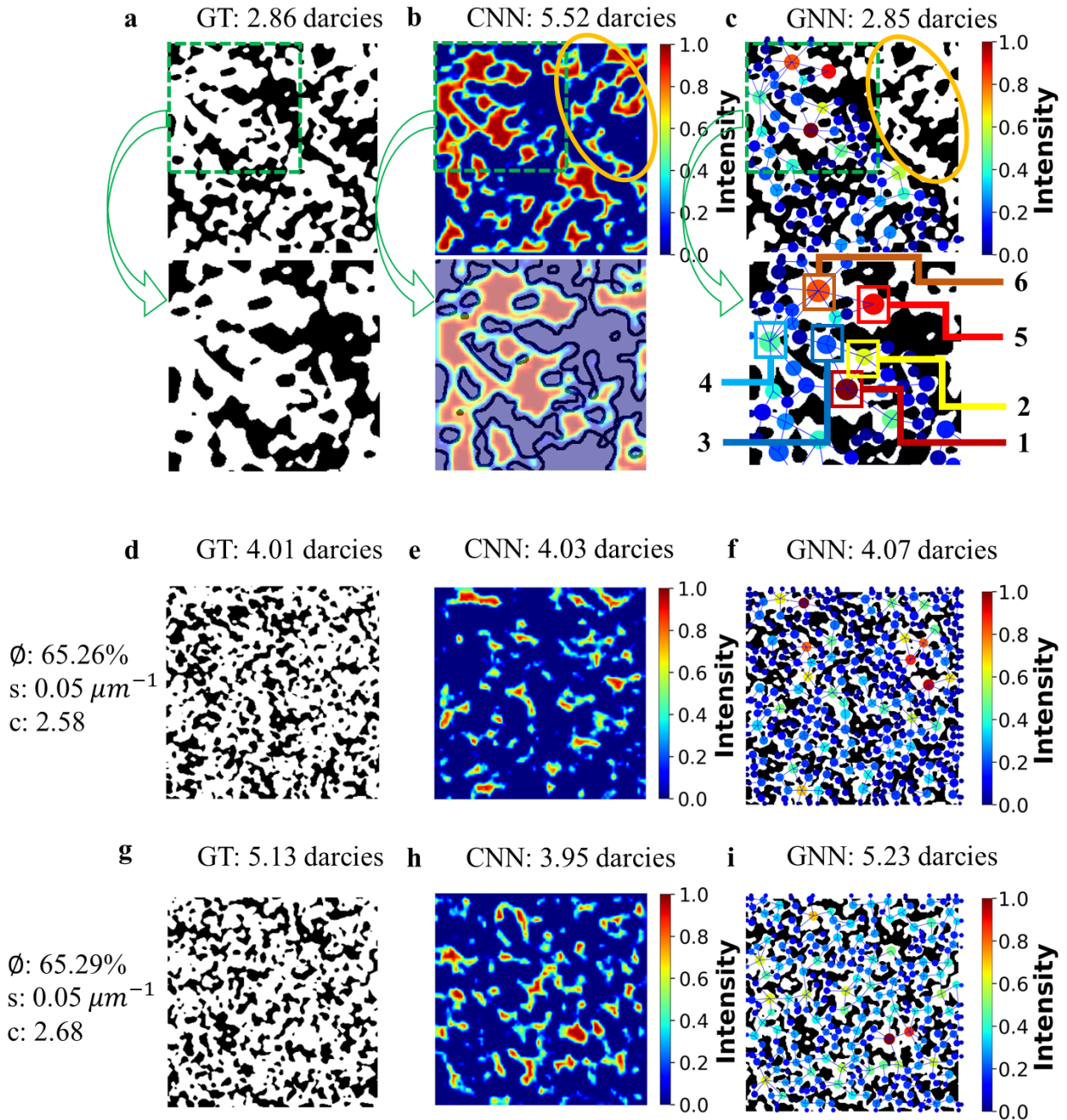


Fig. 4. Grad-CAM-based analysis of CNN and GNN accuracy in predicting permeability across diverse pore geometries. **a** Original 2D image 1. **b** CNN Grad-CAM for image 1. **c** GNN Grad-CAM for image 1. **d** Original 2D image 2. **e** CNN Grad-CAM for image 2. **f** GNN Grad-CAM for image 2. **g** Original 2D image 3. **h** CNN Grad-CAM for image 3. **i** GNN Grad-CAM for image 3.

Discussion

Permeability prediction in rock images presents unique challenges due to the complex and heterogeneous nature of rock microstructures. Among the methodologies explored, the CNN model has emerged as a potent tool, especially adept at processing 3D images. By scanning the pore structure images using filters, CNNs capture local patterns that are crucial for analyzing characteristics like pore shapes and grain boundaries in rock images. This capability to automatically learn and identify these features without explicit manual feature engineering highlights its strength. However, through our in-depth exploration using Grad-CAM, we've illuminated the inherent limitations of the CNN mechanism. Although CNN can learn higher-level characteristics with the convolutional layers going deeper, it might not inherently comprehend some global features, such as pore connectivity and flow pathways.

On the other end, we present a novel GNN approach in this study. Rather than using conventional pixel-level representations of digital rock images, this model is based on a graph-based representation of digital rock graphs. This method offers a more memory-efficient approach, achieved by consolidating clusters of pixels into nodes or edges representing pores and throats. The different prediction performance between the CNN and GNN models can be attributed to their foundational difference in handling spatial or relational data. GNNs are designed to understand relationships between nodes. By capturing the essence of how each pore is related to its neighbors, they offer insights into flow pathways, connectivity, and collective behavior in porous media. This comprehension of fluid movement, driven by the unique properties of pores, is enhanced by our novel interpretation. By employing the novel GNN Grad-CAM technology, we have shed unprecedented light on GNN's intricate mechanisms and their prowess in understanding porous media dynamics.

A key outcome of the present study is the introduction of a fusion model, an innovative methodology that adeptly leverages the strengths of both CNN and GNN for multiscale feature extraction. This integration seamlessly combines CNN's prowess in handling intricate spatial details with GNN's capability to capture complex relational data. Our results strongly affirm that this combined approach not only bridges the gaps inherent in the individual models but also surpasses them in terms of overall predictive accuracy. Significantly, the fusion model represents a pioneering effort in the realm of porous media property predictions, being the first to cohesively integrate 3D digital rock representations. This integration, grounded in rigorous research and methodological innovation, opens avenues for more nuanced and accurate predictions in future studies. The success of this model underscores the potential of hybrid neural network architectures to exceed current limits in digital rock physics and related fields.

Methods

The graph representation for porous media

In the GNN model, porous media is represented using graphs. Graphs are becoming more and more ubiquitous in data science applications and have shown remarkable efficacy in modeling and interpreting unstructured data. They are commonly used to represent diverse datasets, such as intricate patterns in social networks, molecular structures in chemistry, and dynamic flows within traffic networks. A typical graph structure consists of nodes and edges. Nodes represent entities or individual data points, and edges denote the relationships or connections between these entities. In the context of our model, as visualized in Fig. 1b, the graph provides a detailed planar representation of the porous media. Each node corresponds to a specific pore within the

porous medium, and the connecting edges denote the throats—the narrow passages or channels between pores.

The feature of each node in the graph contains 5 properties of the corresponding pore:

1. Pore volume: The space or void within the pore.
2. Pore equivalent diameter: A calculated diameter that represents the size of a pore based on its volume.
3. Pore inscribed diameter: The diameter of the largest circle that can fit inside the pore.
4. Pore extended diameter: A measure that takes into account possible extensions or irregularities of the pores.
5. Pore surface area: The total external surface of the pore.

The feature of each edge in the graph contains 6 properties of the corresponding throat:

1. Throat inscribed diameter: The diameter of the largest circle that can fit within the throat.
2. Throat total length: A measure of the entire length of the throat.
3. Throat direct length: The shortest path or straight-line distance within the throat.
4. Throat perimeter: The boundary length of the throat.
5. Throat cross sectional area: Represents the area available for the flow within the throat.
6. Throat equivalent diameter: A calculated diameter representing the size of the throat based on its cross-sectional area.

An essential feature of our model is the bidirectionality of the edges, ensuring that information is not just passed in a single direction but can flow both ways between nodes. This bidirectional flow facilitates a more robust and comprehensive understanding of the interconnectedness and interactions within the porous media.

Details for CNN and GNN models

In our study, both the 2DCNN and 3DCNN share a structurally similar model design, with the primary distinction being the input dimension. To ensure clarity and succinctness, we focus on the architecture of the 3DCNN. The model, constructed using the PyTorch framework, is hierarchical, incorporating alternating convolutional layers and pooling operations, and culminates in fully connected layers for the output. The core architecture can be observed in Table 3.

Table 3 3DCNN Model Architecture

Layer Type	Input Dimension	Kernel Size	Activation Function	Output Dimension
Convolutional	256×256×256×1	3×3×3	ReLU	256×256×256×3
Max-Pooling	256×256×256×3	2×2×2	-	128×128×128×3
Convolutional	128×128×128×3	3×3×3	ReLU	128×128×128×6
Max-Pooling	128×128×128×6	2×2×2	-	64×64×64×6
Convolutional	64×64×64×6	3×3×3	ReLU	64×64×64×12
Max-Pooling	64×64×64×12	2×2×2	-	32×32×32×12
Flatten	32×32×32×12	-	-	393,216
Dropout	393,216	-	-	393,216
Fully Connected	393,216	-	ReLU	128 nodes
Fully Connected	128 nodes	-	ReLU	64 nodes
Output Layer	64 nodes	-	-	1 node

In the presented work, we built a GNN constructed using the Deep Graph Library (DGL)³⁴. The architecture predominantly consists of a graph convolution layer, an advanced readout mechanism, and a final prediction mechanism. For the graph convolution layer, the process begins with message computation. The message from node u to node v is formulated as:

$$m_{u \rightarrow v} = \text{ReLU} \left(W_{msg} \cdot \left[h_u^{(i-1)}; h_{(u,v)}^{(i-1)} \right] \right) \quad (3)$$

where $h_u^{(i-1)}$ signifies the feature vector of node u from the prior layer, $h_{(u,v)}^{(i-1)}$ represents the edge feature from u to v , W_{msg} is the weight matrix guiding message computation, and “;” indicates concatenation. Following this, the node update mechanism is invoked. The subsequent feature vector of node v is determined by aggregating messages from its neighboring nodes and its previous feature. This can be expressed as:

$$h_v^{(i)} = ReLU\left(W_{apply} \cdot \left[h_u^{(i-1)}; \sum_{u \in N(v)} m_{u \rightarrow v}\right]\right) \quad (4)$$

where W_{apply} serves as the weight matrix for node updates. Subsequent to convolution operations, the readout mechanism is employed. Node embeddings, from the terminal convolution layer, are processed through a readout function, utilizing a weighted summation and aggregation approach. The weighted sum of node features for the entire graph, denoted as $h_g^{(sum)}$, is defined as:

$$h_g^{(sum)} = \sum_{v \in G} w_v \cdot h_v \quad (5)$$

where w_v stands for the weight assigned to node v , which is derived using an atom weighting neural network and G represents the graph. The mean of node features for the entire graph, denoted as $h_g^{(mean)}$, is then given by:

$$h_g^{(mean)} = \frac{1}{|G|} \sum_{v \in G} h_v \quad (6)$$

where $|G|$ denotes the total number of nodes in the graph. The subsequent graph feature vector, named h_g , is defined as:

$$h_g = \left[h_g^{(sum)}; h_g^{(mean)}\right] \quad (7)$$

Lastly, the prediction mechanism employs the graph representation h_g for the further transformation. The intermediate graph features $h_{intermediate}$ and the final output can be described by the following equations:

$$h_{intermediate} = ReLU \left(BatchNorm \left(W_1 \cdot Dropout(h_g) \right) \right) \quad (8)$$

$$output = W_2 \cdot h_{intermediate} \quad (9)$$

where W_1 and W_2 are matrices corresponding to the primary and secondary linear transformation layers, respectively. The *Dropout* layer, an optional regularization mechanism, can be fine-tuned during model initialization to avert overfitting. The *BatchNorm* symbolizes the batch normalization operation, advocating for model stability and enhanced convergence rate. Through this method, the GNN integrates information from the digital rock graph, encompassing both pores and throats, culminating in a comprehensive graph representation.

Grad-CAM

Grad-CAM is a technology designed to provide visual explanations for decisions made by deep learning models, particularly for CNNs. In the CNN models, we chose the final convolutional layers as the target for Grad-CAM, given that these layers typically contain higher-level features, capturing more abstract representations of the inputs. By focusing on these layers, Grad-CAM visualizes what abstract features or patterns influence the model's decision most. The workflow of the CNN Grad-CAM is illustrated in Fig. 5a. First, two hooks, forward and backward, are registered to the chosen target layer. The forward hook captures the activations when data passes through the layer during the forward pass. On the other hand, the backward hook captures the

gradients during the backpropagation process. When an image batch passes through the model, the hooks become active. The forward hook saves the feature activations of the target layer, while the backward hook saves its gradients. The activations are the feature maps that represent the learned patterns, and the gradients represent the rate of change of the output with respect to these feature maps. For each feature map in the target layer, the gradients are spatially averaged, yielding a set of weights. These weights indicate the importance of each feature map regarding the model's prediction. The Class Activation Map (CAM) is generated by taking a weighted combination of the feature maps using the computed weights. The resulting CAM undergoes a ReLU activation to ensure only the positive influences (regions enhancing the prediction) are retained. Following the application of the ReLU activation to the weighted combination of feature maps, a normalization step was implemented. This normalization rescaled the resulting heatmap values between 0 and 1, ensuring a consistent visual representation and emphasizing the regions of importance. This normalization aids in providing a clearer contrast between significant and non-significant regions, enhancing the interpretability of the highlighted areas in the context of rock image permeability prediction. The final CAM, which acts as a heatmap, is overlaid on the original grayscale rock image. This superimposition allows for a clear visual representation of the regions in the rock image that the model deemed significant when predicting permeability. Through the application of Grad-CAM to the hidden layers, we provided a window into the inner workings of the CNN. By focusing on the intermediate layers, it offers a more nuanced insight into how the model discerns and uses intricate patterns in rock images to arrive at its permeability predictions.

Unlike CNNs, GNNs do not process images but graphs. The GNN Grad-CAM should highlight the nodes that are most influential in the model's prediction. Therefore, a customized

adaptation was made for GNN Grad-CAM, as shown in Fig. 5b. First, we performed a forward pass through the model while keeping track of the node embeddings and enabling gradient computation for the input features. Then, a backward pass is done from a target node or the node with the highest prediction score. The gradient of the node embeddings is computed and used to get importance weights for each node. These importance weights can be visualized on top of images to get an idea of which parts of the graph (or which nodes) are crucial for the model's predictions. The result differences between CNN and GNN is the gradient source. For CNN, gradients are taken with respect to the output of a particular convolutional layer. For GNN, gradients are with respect to node embeddings after passing through GNN layers. For visualization, we plotted the PNM and overlaid it into the original image, the GNN Grad-CAM scores were set as the different color for each pore.

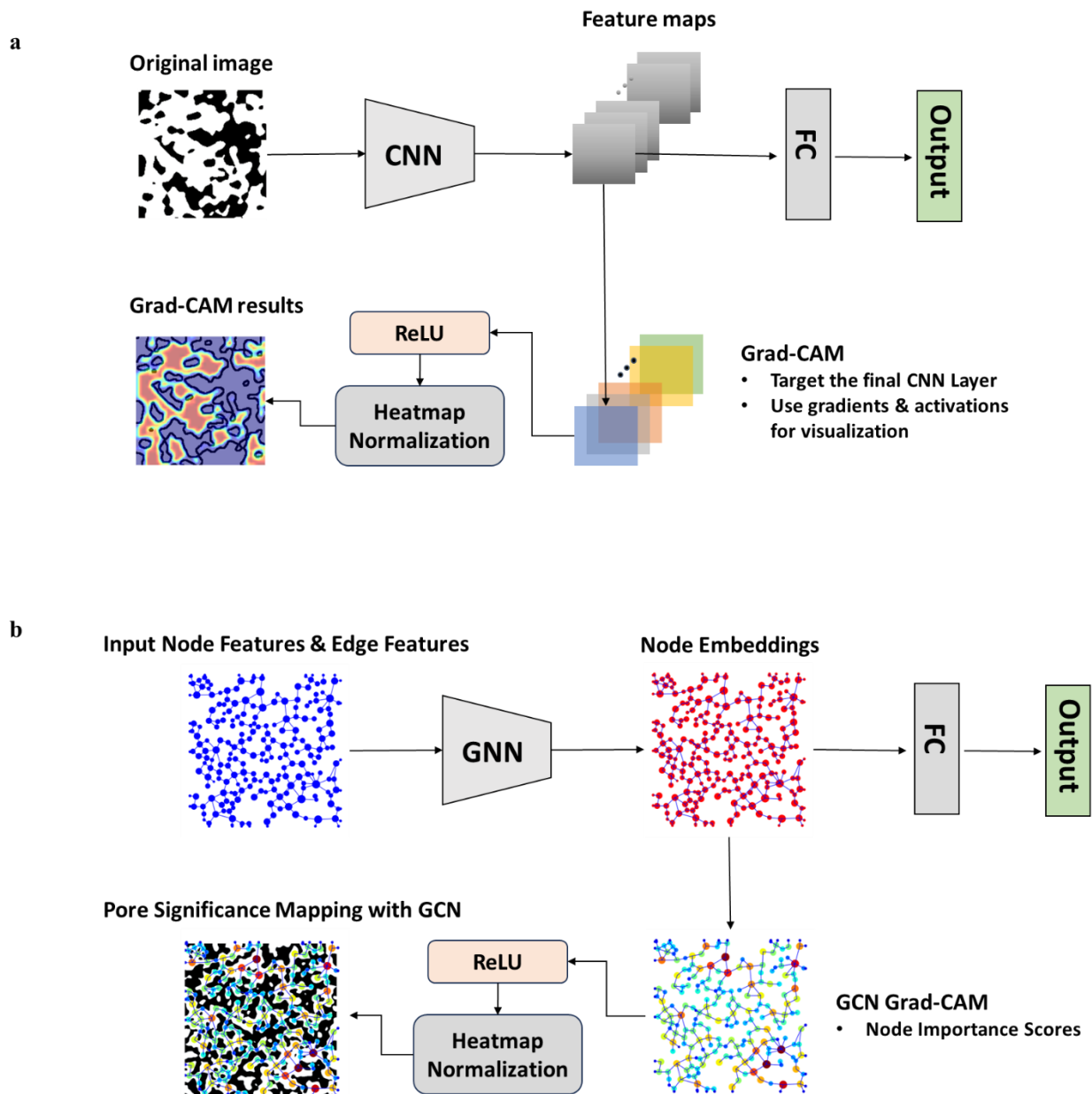


Fig. 5. Visualization workflows using Grad-CAM for CNNs and GNNs. a Workflow of Grad-CAM applied to CNNs, highlighting regions in the input image that significantly influence the model's prediction. **b** Workflow of Grad-CAM adapted for GNNs, emphasizing the nodes in the graph crucial for the model's predictions.

Declaration of Competing Interest

The authors declare that they have no known competing financial interests or personal relationships that could have appeared to influence the work reported in this paper.

Data availability

All data generated or analyzed during this study are available from the corresponding author on reasonable requests.

Code availability

The code for CNN and GNN models is shared on GitHub: <https://github.com/qingqi-code/GNN-PNM>

Acknowledgements

The authors are thankful to the financial support provided by the U.S. Department of Energy (DOE)'s Nuclear Energy University Program (NEUP) through the Award Number of DE-NE0009160.

References

1. Guo, R. *et al.* A Novel Experimental Study on Density-Driven Instability and Convective Dissolution in Porous Media. *Geophysical Research Letters* **48**, e2021GL095619 (2021).
2. Teng, Y., Wang, Y., Li, Z., Qiao, R. & Chen, C. Temperature effect on non-Darcian flow in low-permeability porous media. *Journal of Hydrology* **616**, 128780 (2023).
3. McCarthy, J. F. & Zachara, J. M. Subsurface transport of contaminants. *Environ. Sci. Technol.* **23**, 496–502 (1989).
4. Zhao, B. *et al.* Comprehensive comparison of pore-scale models for multiphase flow in porous media. *Proceedings of the National Academy of Sciences* **116**, 13799–13806 (2019).
5. Zhang, D., Zhang, R., Chen, S. & Soll, W. E. Pore scale study of flow in porous media: Scale dependency, REV, and statistical REV. *Geophysical Research Letters* **27**, 1195–1198 (2000).
6. Blunt, M. J. *et al.* Pore-scale imaging and modelling. *Advances in Water Resources* **51**, 197–216 (2013).

7. Guo, R. *et al.* The role of the spatial heterogeneity and correlation length of surface wettability on two-phase flow in a CO₂-water-rock system. *Advances in Water Resources* **146**, 103763 (2020).
8. LeCun, Y., Bengio, Y. & Hinton, G. Deep learning. *Nature* **521**, 436–444 (2015).
9. Nguyen, P. C. H. *et al.* PARC: Physics-aware recurrent convolutional neural networks to assimilate meso scale reactive mechanics of energetic materials. *Science Advances* **9**, eadd6868 (2023).
10. Alqahtani, N. J. *et al.* Flow-Based Characterization of Digital Rock Images Using Deep Learning. *SPE Journal* **26**, 1800–1811 (2021).
11. Hong, J. & Liu, J. Rapid estimation of permeability from digital rock using 3D convolutional neural network. *Comput Geosci* **24**, 1523–1539 (2020).
12. Tembely, M., AlSumaiti, A. M. & Alameri, W. A deep learning perspective on predicting permeability in porous media from network modeling to direct simulation. *Comput Geosci* **24**, 1541–1556 (2020).
13. Mudunuru, M. K., Cromwell, E. L. D., Wang, H. & Chen, X. Deep learning to estimate permeability using geophysical data. *Advances in Water Resources* **167**, 104272 (2022).
14. Kamrava, S., Tahmasebi, P. & Sahimi, M. Linking Morphology of Porous Media to Their Macroscopic Permeability by Deep Learning. *Transp Porous Med* **131**, 427–448 (2020).
15. Liu, M., Ahmad, R., Cai, W. & Mukerji, T. Hierarchical Homogenization With Deep-Learning-Based Surrogate Model for Rapid Estimation of Effective Permeability From Digital Rocks. *Journal of Geophysical Research: Solid Earth* **128**, e2022JB025378 (2023).
16. Wang, Y. D., Blunt, M. J., Armstrong, R. T. & Mostaghimi, P. Deep learning in pore scale imaging and modeling. *Earth-Science Reviews* **215**, 103555 (2021).

17. Tang, P., Zhang, D. & Li, H. Predicting permeability from 3D rock images based on CNN with physical information. *Journal of Hydrology* **606**, 127473 (2022).
18. Elmorsy, M., El-Dakhakhni, W. & Zhao, B. Generalizable Permeability Prediction of Digital Porous Media via a Novel Multi-Scale 3D Convolutional Neural Network. *Water Resources Research* **58**, e2021WR031454 (2022).
19. Wu, J., Yin, X. & Xiao, H. Seeing permeability from images: fast prediction with convolutional neural networks. *Science Bulletin* **63**, 1215–1222 (2018).
20. Bronstein, M. M., Bruna, J., LeCun, Y., Szlam, A. & Vandergheynst, P. Geometric Deep Learning: Going beyond Euclidean data. *IEEE Signal Processing Magazine* **34**, 18–42 (2017).
21. Zhou, J. *et al.* Graph neural networks: A review of methods and applications. *AI Open* **1**, 57–81 (2020).
22. Kipf, T. N. & Welling, M. Semi-Supervised Classification with Graph Convolutional Networks. Preprint at <https://doi.org/10.48550/arXiv.1609.02907> (2017).
23. Chen, C. *et al.* Optimization of Lattice Boltzmann Simulation With Graphics-Processing-Unit Parallel Computing and the Application in Reservoir Characterization. *SPE Journal* **21**, 1425–1435 (2016).
24. Hamilton, W. L., Ying, R. & Leskovec, J. Inductive Representation Learning on Large Graphs. Preprint at <https://doi.org/10.48550/arXiv.1706.02216> (2018).
25. Vashishth, S., Sanyal, S., Nitin, V. & Talukdar, P. Composition-based Multi-Relational Graph Convolutional Networks. Preprint at <https://doi.org/10.48550/arXiv.1911.03082> (2020).
26. Wu, Z. *et al.* A Comprehensive Survey on Graph Neural Networks. *IEEE Transactions on Neural Networks and Learning Systems* **32**, 4–24 (2021).

27. Jones, D. *et al.* Improved Protein–Ligand Binding Affinity Prediction with Structure-Based Deep Fusion Inference. *J. Chem. Inf. Model.* **61**, 1583–1592 (2021).
28. Li, S., Zhou, J., Xu, T., Dou, D. & Xiong, H. GeomGCL: Geometric Graph Contrastive Learning for Molecular Property Prediction. *Proceedings of the AAAI Conference on Artificial Intelligence* **36**, 4541–4549 (2022).
29. Reiser, P. *et al.* Graph neural networks for materials science and chemistry. *Commun Mater* **3**, 1–18 (2022).
30. Blunt, M. J. Flow in porous media — pore-network models and multiphase flow. *Current Opinion in Colloid & Interface Science* **6**, 197–207 (2001).
31. Rabbani, A., Babaei, M., Shams, R., Wang, Y. D. & Chung, T. DeePore: A deep learning workflow for rapid and comprehensive characterization of porous materials. *Advances in Water Resources* **146**, 103787 (2020).
32. Selvaraju, R. R. *et al.* Grad-CAM: Visual Explanations from Deep Networks via Gradient-Based Localization. in *2017 IEEE International Conference on Computer Vision (ICCV)* 618–626 (2017). doi:10.1109/ICCV.2017.74.
33. Kruczek, B. Carman–Kozeny Equation. in *Encyclopedia of Membranes* (eds. Drioli, E. & Giorno, L.) 1–3 (Springer, 2015). doi:10.1007/978-3-642-40872-4_1995-1.
34. Wang, M. *et al.* Deep Graph Library: A Graph-Centric, Highly-Performant Package for Graph Neural Networks. *arXiv.org* <https://arxiv.org/abs/1909.01315v2> (2019).